

VLM4VLA: REVISITING VISION-LANGUAGE-MODELS IN VISION-LANGUAGE-ACTION MODELS

Jianke Zhang¹, Xiaoyu Chen¹, Qiuyue Wang², Mingsheng Li², Yanjiang Guo¹, Yucheng Hu¹
 Jiajun Zhang², Shuai Bai², Junyang Lin², Jianyu Chen¹

¹ Institute for Interdisciplinary Information Sciences, Tsinghua University

² Qwen Team, Alibaba Inc. 

ABSTRACT

Vision-Language-Action (VLA) models, which integrate pretrained large Vision-Language Models (VLMs) into their policy backbone, are gaining significant attention for their promising generalization capabilities. This paper revisits a fundamental yet seldom systematically studied question: how VLM choice and competence translate to downstream VLA policies performance? We introduce **VLM4VLA**, a minimal adaptation pipeline that converts general-purpose VLMs into VLA policies using only a small set of new learnable parameters for fair and efficient comparison. Despite its simplicity, VLM4VLA proves surprisingly competitive with more sophisticated network designs. Through extensive empirical studies on various downstream tasks across three benchmarks, we find that while VLM initialization offers a consistent benefit over training from scratch, a VLM’s general capabilities are poor predictors of its downstream task performance. This challenges common assumptions, indicating that standard VLM competence is necessary but insufficient for effective embodied control. We further investigate the impact of specific embodied capabilities by fine-tuning VLMs on seven auxiliary embodied tasks (e.g., embodied QA, visual pointing, depth estimation). Contrary to intuition, improving a VLM’s performance on specific embodied skills does not guarantee better downstream control performance. Finally, modality-level ablations identify the visual module in VLM, rather than the language component, as the primary performance bottleneck. We demonstrate that injecting control-relevant supervision into the vision encoder of the VLM yields consistent gains, even when the encoder remains frozen during downstream fine-tuning. This isolates a persistent domain gap between current VLM pretraining objectives and the requirements of embodied action-planning.

1 INTRODUCTION

Vision-Language-Action (VLA) models (Brohan et al., 2023) have recently emerged as a central research focus, as they leverage the extensive visual-language knowledge from Vision-Language Models (VLMs) as a prior for enhancing the generalization of robotic strategies (Kim et al., 2024; Black et al., 2024; Zhang et al., 2024; Chen et al., 2025c). The majority of existing VLA methods have focused on developing more advanced network architectures (Li et al., 2023; Shi et al., 2025), incorporating additional training paradigms or modalities (Zheng et al., 2024; Chen et al., 2024; Zhang et al., 2025a), and refining action decoding schemes (Zhao et al., 2023; Pertsch et al., 2025; Wen et al., 2025). However, limited attention (Liu et al., 2025) has been given to a fundamental question at the core of VLA: how do the choice and specific capabilities of the underlying VLM affect the performance of VLA policies?

In this paper, we revisit this crucial problem. To provide a fair and clean test interface that evaluates the capabilities of VLMs without introducing extraneous variables, we first build the generic **VLM4VLA** pipeline to convert general-purpose VLMs into VLAs, as shown in Figure 2. VLM4VLA is a carefully designed network plug-in, introducing fewer than 1% new parameters. To enhance the stability of inference and the robustness of evaluation, we use a simple MLP head with L1/L2 loss rather than a diffusion-based (flow-matching) approach, thus controlling stochasticity and reducing

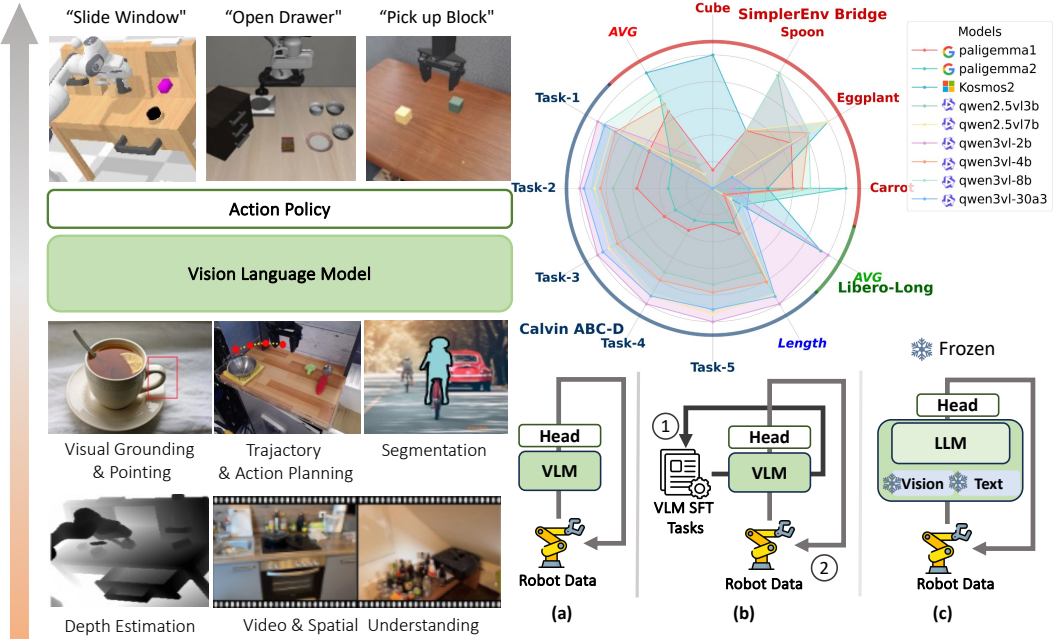


Figure 1: An overview of our **VLM4VLA** framework. **(Left)** The evaluation pipeline for testing different VLM backbones, which are evaluated on downstream tasks after an optional fine-tuning stage on auxiliary embodied tasks. **(Bottom Right)** We systematically investigate three factors influencing VLM-to-VLA transfer: the choice of VLM backbone, the impact of fine-tuning on auxiliary embodied tasks, and the influence of different training strategies (frozen vs. fine-tuned different VLM modules, training from scratch). **(Top Right)** A visualization of inconsistent performance of various VLM backbones across downstream tasks.

tuning complexity. This network allows us to train the modified VLMs directly using downstream robot data, facilitating alignment between the VLM’s capabilities and the demands of robotic tasks. Despite its simplicity, VLM4VLA proves effective, demonstrating competitive performance against more advanced network designs, such as the flow-matching action expert (Black et al., 2024), on benchmark tests. This provides a solid foundation for conducting fair and scalable experiments across various VLMs, aligning their capabilities with the demands of embodied tasks.

Based on the VLM4VLA pipeline, we conduct a large-scale empirical study across various downstream tasks on three commonly used benchmarks, evaluating 24 different VLMs that are either zero-shot or fine-tuned. Specifically, we investigate the VLM capabilities across three dimensions:

- **General capability.** We first quantify the benefit of VLM pretraining by comparing VLM-initialized policies against each other and training-from-scratch baselines. We then examine whether a VLM’s general-purpose strength (as measured by standard VLM evaluations) predicts its downstream embodied control performance.
- **Embodied-specific capability.** Recent works have sought to enhance VLAs by improving the VLM backbone on a series of VLM tasks. We examine how the embodied-specific capabilities of VLMs correlate with performance on downstream control tasks.
- **Modality-level Analysis.** Finally, we disentangle the contributions of each modality by independently ablating the vision and language encoders. We compare freezing versus fine-tuning each module to assess whether further aligning pretrained representations with control-relevant information improves downstream VLA performance.

For general capability, we select nine open-sourced VLMs as the backbone. As shown in Figure 1 (a), we apply the VLM4VLA pipeline directly to these VLMs together with the training from scratch baselines and fine-tune them with robot data. For embodied-specific capability, we collect seven commonly used embodied tasks or pretrained models based on the Qwen2.5-VL (Bai et al., 2025b) backbone to conduct ablation studies. As shown in Figure 1 (b), we either fine-tune the

VLM using auxiliary datasets or directly use the released fine-tuned models. We then apply the VLM4VLA pipeline to adapt these models to the embodied policies. Lastly, we conduct modality-level ablations to disentangle the contributions of vision and language components (Figure 1 (c)). This involves selectively freezing or fine-tuning the vision and text encoders. Furthermore, we investigate the efficacy of injecting control-specific knowledge directly into the vision encoder via the FAST tokenizer (Pertsch et al., 2025). We evaluate the fine-tuned models on a range of tasks across three benchmarks including Calvin (Mees et al., 2022), SimplerEnv (Li et al., 2024), and Libero (Liu et al., 2023) to assess their embodied capabilities.

To our surprise, our findings reveal that while VLM initialization offers a consistent benefit over training from scratch, a VLM’s general capabilities are poor predictors of its downstream task performance, contrary to common assumptions. For instance, we observe that Kosmos (Peng et al., 2023) outperforms Qwen2.5-VL (Bai et al., 2025b) and Paligemma (Steiner et al., 2024) in certain environments. Inconsistencies across benchmarks suggest that VLA policies require capabilities beyond those currently pursued by VLMs. Furthermore, the gains by fine-tuning VLMs on specific auxiliary embodied tasks do not transfer to the downstream control tasks. Lastly, our modality-level analysis identifies the vision encoder, rather than the language component, as the primary performance bottleneck. We find that fine-tuning the vision encoder is essential for strong control performance, whereas the language encoder is less critical. The significant performance gains observed after injecting action-relevant information into the vision modules within the VLM confirm the existence of a critical domain gap between standard VLM pretraining and the visual representation requirements of embodied tasks.

Taken together, these results indicate a significant gap between current VLM research and the practical demands of VLA models. We believe this work highlights the fundamental question of the VLM’s role in embodied agents and can help guide future exploration in this area.

2 RELATED WORKS

Vision-Language-Action Models Recent works are increasingly focusing on introducing Vision-Language-Models (VLMs) (Dai et al., 2024; Touvron et al., 2023; Wang et al., 2025a; Bai et al., 2025b) into robot policies to enhance their generalization capabilities (Brohan et al., 2023; Guo et al., 2025; Hu et al., 2024; Guo et al., 2024), which are known as Vision-Language-Action (VLA) models. Early methods like RT-2 (Brohan et al., 2023) and OpenVLA (Kim et al., 2024) discretized actions into language tokens, enabling action learning through the VLM’s autoregressive framework. Subsequent works have utilized policy heads to decode continuous actions, gradually evolving the VLA design into a hierarchical structure that combines a VLM with a policy head (Black et al., 2024; Zhang et al., 2024; Cui et al., 2025). However, most prior works focused on constructing complex policy networks, while overlooking the impact of the VLM backbone itself on the overall VLA performance. Though RoboVLMs (Liu et al., 2025) compared the influence of a few early VLM backbones, it did not ensure consistency in its implementations. In contrast, we design a fairer experimental framework to comprehensively test the impact of various advanced VLMs across multiple environments. By employing the simplest and a consistent additional action policy, we minimize the influence of the policy head component on the experimental results.

Embodied Tasks for VLM Many prior works have explored introducing embodiment-related tasks into Vision-Language Models to enhance their spatial understanding (Yang et al., 2025; Feng, 2025) and task execution capabilities (Intelligence et al., 2025; Zhou et al., 2025b). These tasks include dense prediction (Wang et al., 2025b; Zhang et al., 2025b) and autoregressive VQA tasks (Rana et al., 2023; Yuan et al., 2024; Sermanet et al., 2024). Recently, inspired by the hierarchical System 1 and System 2 design paradigm (Zhang et al., 2024; Shentu et al., 2024), much research focused on using VLMs to build a general-purpose “robot brain”—a large language model capable of planning or completing real-world tasks via language. For instance, Robo2v1m (Chen et al., 2025b) annotated datasets like Open-X for VQA tasks, while Robobrain (Team, 2025) constructed affordance and visual trace tasks from RoboVQA (Sermanet et al., 2024) and video datasets. Additionally, many VLA studies leverage auxiliary post-training or co-training tasks of VLM (Intelligence et al., 2025; Zhang et al., 2025a) to obtain better backbone networks. In our subsequent experiments, we fine-tune VLM on various post-training tasks and compare its performance as a VLA backbone against the

corresponding VLM baselines, thereby validating the effectiveness of these auxiliary VLM tasks for VLA performance.

3 STUDY DESIGN

To create a comprehensive and fair benchmark of VLM performance on manipulation tasks, we designed the VLM4VLA framework around three core principles:

- **Fairness and Reproducibility** We employ a consistent model architecture and training/testing settings across multiple simulation environments to ensure fair and reproducible comparisons.
- **Minimalist Design** We encapsulate VLMs within a simple yet effective VLA framework, thereby minimizing the influence of complex, extraneous policy designs on the comparison.
- **Isolating Core VLM Capabilities** To directly evaluate the VLM’s intrinsic knowledge, our framework relies exclusively on visual-language inputs. We format input sequences to match each VLM’s native instruction-tuning format and deliberately exclude other modalities like proprioceptive state or tactile feedback. This isolates the VLM’s contribution and directly tests how its intrinsic capabilities translate to manipulation.

In the following sections, we will detail the VLM4VLA research framework. In Sec 3.1 we introduce the basic experimental design. We then describe the model architecture within VLM4VLA in Sec 3.2, and Sec 3.3 explains the experiment setup and evaluation protocol.

3.1 BASIC EXPERIMENT DESIGN

As shown in Figure 1, our objective is to investigate the impact of different VLMs, as well as VLM-specific fine-tuning tasks, on the performance of the resulting VLA. Our experiments primarily focus on VLMs ranging from 1B to 10B parameters, as well as various embodiment-related auxiliary tasks and different training settings of transferring VLM to VLA. Beyond fundamental vision-language alignment, the general capabilities of VLMs relevant to embodied tasks include visual grounding, trajectory and action prediction, task planning, video understanding, and spatial reasoning. Some models also possess image rendering capabilities, such as depth prediction and semantic segmentation, as seen in works like Beyer et al. (2024); Chen et al. (2025a); Deng et al. (2025). To compare the effectiveness of these models and tasks, we encapsulate each VLM—both in its original form and after being fine-tuned on a specific auxiliary task—into a VLA, following the methodology described in Sec 3.2. All VLAs, despite their different backbones, share an identical action encoding and decoding scheme and introduce a minimal number of additional trainable parameters (less than 1%).

Subsequently, these VLM4VLA models are trained on robotic datasets using a consistent training setup. During this process, we fine-tune all model parameters, as our studies in Sec 4.3 demonstrate that freezing parts of the model leads to significant performance degradation. The fine-tuned models are then deployed for rollouts in the target environments, where we measure the success rates on various tasks. The VLA performance is assessed according to the protocol detailed in Sec 3.3.

3.2 VLM4VLA NETWORK DESIGN

In this section, we detail the method for constructing a consistent VLA from various VLMs within the **VLM4VLA** framework, as illustrated in Figure 2. Our objective is to build a VLA architecture that is generic across different VLMs, lightweight, and capable of fully leveraging the VLM’s intrinsic knowledge.

We introduce a learnable action query token to extract embodiment-related knowledge from the VLM. The representation of this token is then decoded into an action chunk. To align with the pre-training input format of each model, we adapt a unique token concatenation scheme for each VLM4VLA instance. We take the

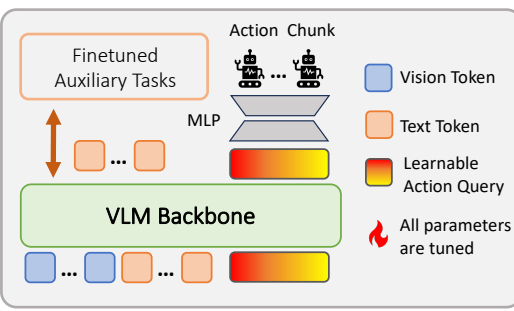


Figure 2: VLA Network in VLM4VLA

$\langle \text{last_hidden_state} \rangle$ of the $\langle \text{ActionQuery} \rangle$ token, as encoded by the VLM, and decode it into an action chunk using a small MLP-based policy head. The overall action output can be formulated as:

$$\text{action} = \text{MLP}(\text{VLM}([\langle \text{img} \rangle \dots \langle \text{img} \rangle \langle \text{text} \rangle \dots \langle \text{text} \rangle \langle \text{ActionQuery} \rangle]))$$

where $\langle \text{img} \rangle$ represents the visual embeddings from the vision encoder, $\langle \text{text} \rangle$ corresponds to the language embeddings containing the instruction and any additional prompts, and $\langle \text{ActionQuery} \rangle$ is the learnable action query token. The token sequence above omits VLM-specific special tokens (e.g. $\langle \text{PAD} \rangle$ or $\langle \text{EOS} \rangle$...) for brevity. Further details can be found in Appendix A.2.

Training Objective During training, we finetune all parameters of the VLM, including the LLM, the vision encoder, and the word embeddings. We deliberately avoid widely-used objectives like diffusion loss and flow-matching loss. Our preliminary experiments revealed that these losses introduce significant stochasticity during inference, requiring a much larger number of rollouts for accurate evaluation. They also cause substantial performance fluctuations between different checkpoints late in training, which is not conducive to the fair comparison we aim to achieve. As a result, we utilize a maximum likelihood imitation learning objective. The desired relative position \mathbf{a}^{pos} of the end-effector (or continuous joint action) is optimized via a modified MSE loss (Huber loss). The discrete status a^{end} of the end-effector is optimized with a binary cross-entropy loss:

$$\mathcal{L} = \frac{1}{|\mathcal{B}|} \sum_{\mathcal{B}} (\|\mathbf{a}^{\text{pos}} - \hat{\mathbf{a}}^{\text{pos}}\|_2^2 + \text{BCE}(a^{\text{end}}, \hat{a}^{\text{end}})) \quad (1)$$

where $\hat{\mathbf{a}}^{\text{pos}}$ and \hat{a}^{end} denote the demonstration data for the relative position and status of the end-effector in a sampled mini-batch \mathcal{B} .

3.3 EXPERIMENT SETTINGS AND EVALUATION PROTOCOL

We fine-tune the VLM and the action policy for each model using identical hyperparameters and model configurations for fair comparisons. We conduct a learning-rate sweep and select a unified hyperparameter configuration to ensure that all models reached convergence at evaluation time (details can be found in Appendix A.2.2). Specifically, the model uses a single-view image of the current frame as its visual input and does not take proprioceptive information; this prevents the model from directly learning actions from the state. To handle inconsistent input image sizes across different VLMs, we standardize the input to 224×224 resolution for all training (an ablation on different image resolutions can be found in Appendix A.2.4). If a VLM requires a different input size, we first process the image at 224×224 and then resize it to the model-specific dimensions. During training, all parameters of VLM are trained, including the vision encoder, word embeddings, LLM, and small policy head. For each VLM, we use a simple instruction prompt consistent with its pre-training format (detailed prompts format for each model can be found in Appendix A.2.3).

To ensure the reproducibility and fairness of our experiments, we do not use real-world tasks for evaluation. A direct consequence of this choice is that it prevents other researchers from directly comparing their own models against our findings on physical robots. We test different models in three simulation environments: Calvin (Mees et al., 2022), SimplerEnv (Li et al., 2024), and Libero (Liu et al., 2023). Since each environment requires separate training and testing, to improve the efficiency and rigor of our evaluation, we select the most challenging scenarios as our evaluation benchmarks. During tests, we experiment with executing the full action chunk, half of the action chunk, and a single step over all validation checkpoints. We report the best-performing result. More details about the settings of different environments can be found in the Appendix A.1.

Calvin ABC-D We evaluate on the Calvin ABC-D task. We train the model for 30k steps on the ABC splits and evaluate it on 1000 task sequences, each with a length of 5. During testing, the policy is required to complete a sequence of 1–5 tasks. This setup challenges the VLM’s ability to generalize to novel visual scenes. We report the average number of successfully completed tasks per sequence.

SimplerEnv Bridge To better differentiate the performance of various VLM-based policies, we choose the WindowX (Bridge V2) task suite, which is more challenging than the Fractal suite. We train for 50k steps on Bridge–V2 (Walke et al., 2023). During evaluation, we run 24 trials with random initializations for each of the four scenes (Pick Carrot, Pick Eggplant, Pick Spoon, and Stack Cube) and calculate the success rate.

Libero-Long (-10) Among the five task suites in Libero, we evaluate different models on the most challenging suite **Libero-Long**, which consists of 10 tasks involving a variety of objects and skills. All models are trained for 50k steps on the training split and evaluated with 50 trials with random initializations for each task.

4 EXPERIMENTS AND ANALYSIS

To comprehensively evaluate how VLM capabilities transfer to robot manipulation, our experimental analysis is four-fold. First, in Sec 4.1, we benchmark various open-source VLMs on a challenging set of tasks across three simulators to assess the relationship between general capability and the downstream performance. Second, in Sec 4.2, we investigate whether improvements gained from finetuning on specific auxiliary embodied tasks translate to better final performance. Then, in Sec 4.3, we analyze the importance of the different modules within VLM by comparing the outcomes of freezing versus fine-tuning it during VLA adaptation. Through the above experiments, we observe a clear gap between VLMs and VLAs, particularly a misalignment in the features produced by the vision encoder. To further investigate the factors underlying this gap, we conduct additional experiments in Sec. 4.4, which indicate that the gap may stem from a mismatch between visual–language tasks and low-level action control tasks. Additionally, in Appendix A.2.5, we report results where the VLA is trained from scratch without any pretrained VLM, providing a lower-bound reference for VLA performance.

4.1 PERFORMANCE OF DIFFERENT VLMs ON VLM4VLA

4.1.1 BASELINES

VLM Baselines We evaluate several Vision-Language Models commonly used in open-source VLAs, with model sizes generally ranging from 1B to 10B parameters (we also incorporate a large 30B-MoE-based VLM to diversify the types of backbone architectures), which ensures the feasibility of extensive action-learning finetuning and rollout testing. We test a variety of VLM models from the VLA domain, including the **Paligemma** series (**paligemma-1** (Beyer et al., 2024) and **paligemma-2** (Steiner et al., 2024)), the **QwenVL** series (**Qwen2.5VL-3B**, **Qwen2.5VL-7B**, **Qwen3VL-2B**, **Qwen3VL-4B**, **Qwen3VL-8B**, **Qwen3VL-30B-A3B**) (Bai et al., 2025b;a) and **Kosmos-2** (Peng et al., 2023). Among these, the **QwenVL** series are top-tier general-purpose open-source VLMs, **Paligemma** is designed for better adaptability to downstream finetuning, and the **Kosmos** series excels at grounding tasks. These models cover a range of multimodal LLMs with diverse architectures and strengths, allowing us to compare their action-learning capabilities comprehensively. Also, to estimate the lower bound of current VLAs, we evaluate several models trained from scratch without any pretrained VLM, providing a lower-bound reference for VLA performance (detailed results can be found in Appendix A.2.5).

VLA Baselines For comparison, we select several expert VLAs as reference baselines, which use different VLMs as their backbones:

- **OpenVLA** (Kim et al., 2024): Uses **Llama2-7B** with **DINOv2/SigLIP** as its VLM backbone. It differs from our VLM4VLA framework by decoding actions into a discrete space. The total model size is approximately 7.7B. For the **Calvin** environment, we report our reproduced OpenVLA results, while for the **Simpler** and **Libero** environments, we report the official results. Similar to our VLM4VLA setup, this model uses only a single image as input and does not leverage proprioceptive state.
- **pi0** (Black et al., 2024): Based on **Paligemma-1**, with a total size of approximately 3.1B. We modify the code provided by *open-pi-zero* to train and test within our setups, ensuring consistent settings with other backbones. We remove the proprioceptive expert and use a single image as input. More details can be found in Appendix A.3.
- **ThinkAct** (Huang et al., 2025): A recent VLA model enhanced with reinforcement learning, based on **Qwen2.5VL-7B**. We report its official results on **Simpler** and **Libero** for comparison against our **Qwen2.5VL-7B** baseline. Unlike other baselines, ThinkAct takes use of proprioceptive state as an input.

4.1.2 MAIN RESULTS

The performance of different VLMs on robotics tasks is presented in Tables 1 and 2. In addition to success rates, we report the number of finetuned parameters for each model in the *size* column. In Table 8 (Appendix A.2.5), we report results where the VLA is trained from scratch without any pretrained VLM, indicating that VLM pre-training is fundamental to the ability of VLA models.

Table 1: Results on Calvin ABC-D. Entries marked with * are expert VLAs modified and reproduced with our training and test settings.

Model (VLM Backbone)	Size	Task-1	Task-2	Task-3	Task-4	Task-5	Calvin↑
<i>Expert Vision-Lanugage-Action Models</i>							
OpenVLA* (Llama-2)	7.7B	0.792	0.644	0.499	0.368	0.245	2.548
pi0* (Paligemma-1)	3.1B	0.896	0.785	0.786	0.610	0.532	3.509
<i>VLM with VLM4VLA Models</i>							
Qwen2.5VL-3B	3.8B	0.922	0.842	0.766	0.700	0.626	3.856
Qwen2.5VL-7B	8.3B	0.935	0.864	0.807	0.758	0.693	4.057
Qwen3VL-2B	2.1B	0.943	0.882	0.831	0.776	0.710	4.142
Qwen3VL-4B	4.4B	0.933	0.857	0.790	0.719	0.644	3.943
Qwen3VL-8B	8.8B	0.940	0.868	0.797	0.746	0.684	4.035
Qwen3VL-30B-A3B	31.1B	0.939	0.877	0.820	0.757	0.682	4.075
Paligemma-1	2.9B	0.914	0.813	0.692	0.599	0.488	3.506
Paligemma-2	3.0B	0.901	0.775	0.669	0.575	0.486	3.406
KosMos-2	1.7B	0.878	0.721	0.591	0.498	0.408	3.096

As shown in Table 1 for the Calvin ABC-D task, QwenVL series models significantly outperform other VLMs. Notably, the average of completed tasks using single view image by Qwen2.5VL-7B, Qwen3VL-2B, Qwen3VL-8B is nearly on par with state-of-the-art VLAs. Furthermore, VLMs that perform better on QA-benchmarks, such as the QwenVL series, also exhibit superior performance on Calvin, suggesting a correlation between the capabilities tested by Calvin and other VQA benchmarks. Concurrently, we observe that pi0, which is based on Paligemma-1 and does not use state information, performs similarly to the base Paligemma-1 model. This indicates that the additional action expert is constrained by the inherent capabilities of VLM backbone itself and fails to yield performance improvements in the Calvin environment.

Table 2: Results on SimplerEnv-Bridge and Libero-10. Entries marked with * are expert VLAs modified and reproduced with our training and test settings.

Model (VLM Backbone)	Size	Carrot	Eggplant	Spoon	Cube	Simpler↑	Libero↑
<i>Expert Vision-Lanugage-Action Models</i>							
OpenVLA (Llama-2)	7.7B	4.2	0.0	0.0	12.5	4.2	53.7
pi0* (Paligemma-1)	3.1B	62.5	100.0	54.2	25.0	60.4	46.0
ThinkAct (Qwen2.5VL-7B)	7.4B	37.5	70.8	58.3	8.7	43.8	70.9
<i>VLM with VLM4VLA Models</i>							
Qwen2.5VL-3B	3.8B	20.8	91.7	79.2	0.0	48.0	43.0
Qwen2.5VL-7B	8.3B	12.5	100.0	75.0	0.0	46.8	45.0
Qwen3VL-2B	2.1B	20.8	95.8	79.2	0.0	49.0	55.8
Qwen3VL-4B	4.4B	54.2	95.8	75.0	0.0	56.3	44.4
Qwen3VL-8B	8.8B	58.3	95.8	79.2	0.0	58.3	46.2
Qwen3VL-30B-A3B	31.1B	29.2	79.2	70.8	0.0	44.8	46.8
Paligemma-1	2.9B	50.0	91.7	75.0	4.2	55.3	44.2
Paligemma-2	3.0B	75.0	75.0	79.2	0.0	57.3	46.2
KosMos-2	1.7B	37.5	100.0	75.0	29.2	60.4	55.0

Table 2 displays the performance of the models on the Simpler-Bridge and Libero-10 (long) tasks. We find that KosMos-2, the smallest model, achieves the highest success rate on both tasks. On the Simpler-Bridge task, the Paligemma series models outperform the Qwen2.5VL series, whereas on Libero-10, the performance across different VLM categories is comparable. It is worth noting that

ThinkAct, finetuned from Qwen2.5VL-7B, performs similarly to the base Qwen2.5VL-7B on Simpler-Bridge. However, its performance on Libero-10 is substantially better than all other models. This may be caused by the proprioceptive state information utilized by ThinkAct, which can be a useful input for Libero environment.

As illustrated in Figure 3, we conducted a linear regression analysis to examine the relationship between VLA performance and the general capabilities of the underlying VLMs. We plot the performance of various VLMs on several general-purpose VQA benchmarks against their performance on VLA tasks.

For Paligemma and Kosmos, we approximated their general capabilities using results from their proprietary tasks. For Qwen-VL, we used the average scores from multiple general-purpose VQA benchmarks. A linear regression line is fitted to visualize the correlation between these two sets of metrics. The results indicate that different evaluation environments exhibit varying degrees of linear correlation with these general VLM capabilities. We found that the results on the Calvin benchmark exhibit a high correlation with performance on VQA benchmarks. In contrast, for the Simpler and Libero environments, there is no apparent correlation between a VLM’s QA performance and its VLA performance. This suggests a significant gap exists between the capabilities required for VLA manipulation tasks and those measured by existing VQA benchmarks. More details about Figure 3 can be found in Appendix A.4.

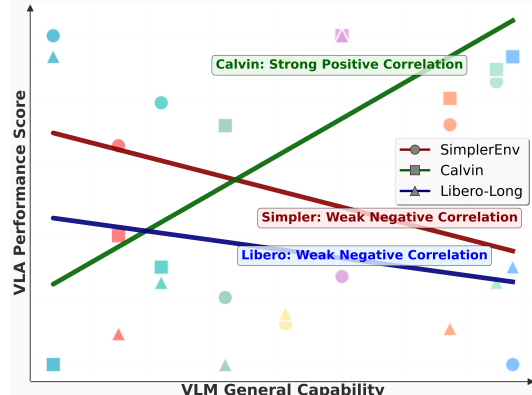


Figure 3: Comparison of the linear relationship between general VLM capabilities and VLA performance.

4.2 IMPACT OF DIFFERENT VLM AUXILIARY TASKS ON VLA PERFORMANCE

Recent works have proposed using robotic data to construct VQA datasets for improving VLM backbones, e.g., Robobrain (Team, 2025). However, few studies have investigated whether this additional continual finetuning actually benefits VLAs in downstream tasks. In this section, we construct or collect several SFT tasks for VLM, including VQA datasets and a generation task. We first finetune the Qwen2.5VL model and subsequently, we employ each finetuned VLM as the backbone for our VLM4VLA framework and evaluate its performance on the Calvin benchmark. Specifically, we compare the following finetuned VLMs (more details about SFT datasets can be found in Appendix A.6):

Robopoint (Yuan et al., 2024) A pointing task dataset collected in simulator. Given an image and a target location, the model is required to output the 2D coordinates that satisfy the target requirement. This finetuning dataset contains 1.432M samples. After finetuning, the performance of Qwen2.5VL-3B on the pointing task improved by $\sim 20\%$ on the test split.

Vica-332k (Feng, 2025) A spatial understanding dataset constructed from RGB-D datasets. It covers a wide range of capabilities, including size estimation, position understanding, distance estimation, and so on. After finetuning Qwen2.5VL-3B on this dataset, we achieve a performance improvement of $\sim 15\%$ on VSI-Bench Yang et al. (2025).

Bridgevqa We used VQASynth to annotate data from Bridge-v2, Fractal, and Calvin ABC, combining them into a spatial understanding question-answering dataset. The main QA content includes judging the distance, size, and depth between two objects.

Robo2v1m (Chen et al., 2025b) An action-oriented question-answering dataset built from 176k real robot trajectories, containing 667k VQA pairs. It involves tasks such as multi-view understanding, success prediction, position management, and trajectory judgment. After finetuning Qwen2.5VL-3B on this dataset, we achieved a 60% performance improvement on its test set.

Robobrain2 (Team, 2025) A large-scale embodied VQA dataset and a VLM finetuned on Qwen2.5VL-7B. The tasks include pointing, planning, and marking trajectory. We directly use their finetuned VLM as the backbone for our VLM4VLA.

Omni-Generation We integrate a diffusion model into Qwen2.5VL-7B and train on both image generation, depth map generation, and semantic segmentation map generation tasks together with general VQA tasks (refer to Qwen-VLo). We use the resulting VLM part as the backbone for VLM4VLA.

VQA-Mix We mix the aforementioned VQA datasets with other large-scale general data to finetune Qwen2.5VL-7B.

Figure 4 presents the performance of the various finetuned VLMs. Overall, all models underperform the original baseline, with most exhibiting a slight degradation in performance and an obvious increase in variance. For Qwen2.5VL-3B, the model finetuned on Vica332k performs better than those finetuned on other datasets. This could be attributed to the dataset’s broad data coverage and diverse task types, which may prevent the model from overfitting to a narrow set of capabilities and consequently degrading others. For Qwen2.5VL-7B, the VQA-Mix model shows the least performance degradation, achieving results nearly identical to the baseline. This suggests that general-purpose VQA data plays a crucial role during embodiment-focused finetuning, further implying that VLAs may require broad, general capabilities, beyond just embodied skills, to perform well on downstream tasks.

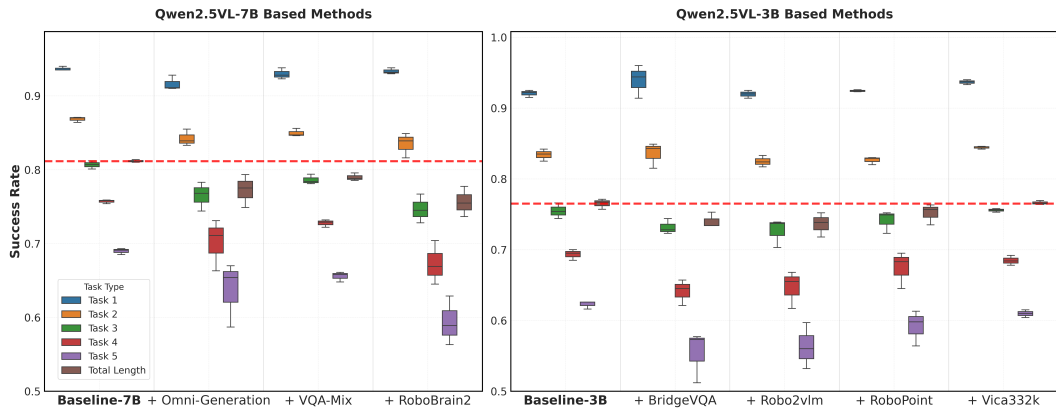


Figure 4: Performance of different auxiliary VLM finetune tasks. The *Total Length* dimension is scaled by a factor of 5 to normalize it to the range [0, 1]. The results for the VLAs trained under each task and for each gradient steps (10k, 15k, 20k, 25k and 30k) are rendered as box plots to provide a view of the impact of different tasks on the VLA’s performance and stability.

It is also worth noting that finetuning with generation tasks (i.e., Omni-Generation on Qwen2.5VL-7B), such as depth and semantic map prediction, did not yield performance benefits. This may indicate that simply introducing generation tasks or dense 3D-aware tasks into VLM finetuning process does not provide a tangible advantage for the VLA. Similarly, Robobrain2, positioned as a general-purpose embodied brain, also underperformed the baseline in our VLM4VLA tests. This suggest that existing embodied VQA-style tasks do not offer a clear benefit for training end-to-end VLAs to execute downstream manipulation tasks. A more in-depth experimental analysis can be found in Sec. 4.4.

4.3 IMPORTANCE OF DIFFERENT VLM MODULES

Table 3 shows the performance of three models when the vision encoder and word embeddings are frozen during VLM4VLA training. We observe a significant performance degradation for all models on both the Calvin and Simpler benchmarks after freezing the vision encoder, with this drop being particularly pronounced for the Paligemma models. In the case of Qwen2.5VL-7B, the vision encoder accounts for 0.7B parameters. When it is frozen, the total number of tunable parameters is still a substantial 7.6B, which is much larger than 3.8B in Qwen2.5VL-3B. However,

the performance of the frozen *Qwen2.5VL-7B* is not only significantly worse than its fully finetuned counterpart but also substantially underperforms the fully finetuned *Qwen2.5VL-3B*.

Table 3: Influence of freezing vision encoder and word embeddings of VLMs

	Size	Calvin ABC-D↑	SimplerBridge↑
Qwen2.5VL-3B	3.8B	3.856	48.00
+ freeze vision encoder	3.1B	2.855 (-1.001)	23.95 (-24.05)
+ freeze word embedding	3.4B	3.849 (-0.007)	46.88 (-1.12)
Qwen2.5VL-7B	8.3B	4.057	46.75
+ freeze vision encoder	7.6B	2.823 (-1.234)	25.50 (-21.25)
+ freeze word embedding	7.8B	3.874 (-0.183)	48.96 (+2.21)
Paligemma-1	2.9B	3.506	55.25
+ freeze vision encoder	2.5B	0.495 (-3.011)	13.25 (-42.00)
+ freeze word embedding	2.7B	3.485 (-0.021)	52.25 (-3.00)

In contrast to the vision-related findings, the ablation on word embeddings shows a different pattern: whether the word embeddings are trained or kept fixed has no noticeable impact on VLA performance.

This finding strongly suggests that finetuning the vision encoder is crucial when adapting a VLM into a VLA, and that the impact of this module can be more significant than merely increasing the number of trainable parameters in the language model. A potential reason for this phenomenon is that the VLM’s pre-trained vision encoder is not well-aligned with the visual domain of embodied scenes. The model likely requires significant adaptation of its vision module to effectively process and align with the visual signals from these novel environments. In the next section (Sec. 4.4), we present additional experiments to hypothesize and validate why the vision component is crucial—an inquiry we also view as a promising direction for future research.

4.4 ANALYSIS OF THE VISUAL GAP BETWEEN VLM AND VLA

In Sec. 4.3, we observe that, relative to other VLM components, the vision encoder has an especially pronounced impact on VLA performance. This indicates a substantial mismatch between the intrinsic visual representations learned by VLMs pretrained on large-scale web image–text corpora and the visual signals required in manipulation settings. By analyzing the characteristics of these two task families, we hypothesize that the visual gap may stem from the following two factors:

1. Real images vs. simulated renderings (Real to Sim): During pretraining, VLMs are exposed to relatively few tabletop simulation renderings. As a result, the vision encoder (e.g., ViT) may lack effective high-level semantic representations for simulated images encountered in manipulation.
2. Vision-language understanding vs. low-level action control: The visual features encoded by the VLM’s vision encoder are better aligned with language-output objectives typical of QA-style tasks, whereas low-level action control in robotics requires different visual cues and representations.

The existence of the real-to-sim gap in point (1) is evident, but it does not fully explain our results across the three simulation-based experiments. Specifically, consider the findings on Simpler-Bridge: we fine-tune the VLA on the real-world BridgeV2 Walke et al. (2023) dataset and evaluate in simulation, yet freezing the vision encoder still leads to a marked drop in performance. This suggests that factor (2) is also likely a key contributor—namely, the need to learn control-specific information (such as low-level actions) that is not captured during general web-scale pretraining. Therefore, we conduct a new experiment to address this question: *Does the vision encoder require fine-tuning merely to bridge the visual gap (Real → Sim), or is there a mismatch between VLM understanding features and robot control features?*

We utilize the BridgeV2 dataset, which consists entirely of real-world images. Following the procedure in Sec. 4.2, we introduce a new VLM fine-tuning task to inject the control-related information into the VLM backbone on real-world images. Inspired by Intelligence et al. (2025); Driess et al. (2025), we encode BridgeV2 actions into discrete tokens using Fast-Token Pertsch et al.

Table 4: Impact of injecting action information during VLM fine-tuning on VLA performance. We compare three settings of VLM finetuning: 1. *Baseline*: without finetuning the VLM at all; 2. *Freeze Vision FT*: Fine-tuning only the LLM (keeping the vision encoder frozen); 3. *Unfreeze Vision FT*: Fine-tuning both the LLM and the vision encoder. These modified VLM backbones are then trained into a standard VLM4VLA policy with frozen or unfrozen vision encoder.

Qwen3VL-4B	SimplerBridge \uparrow	Qwen3VL-4B	SimplerBridge \uparrow
<i>Freeze</i> vision encoder during training VLA		<i>Unfreeze</i> vision encoder during training VLA	
Baseline	27.6	Baseline	56.3
Freeze Vision FT	28.0 (+0.4)	Freeze Vision FT	56.3 (+0.0)
Unfreeze Vision FT	45.7 (+18.1)	Unfreeze Vision FT	59.4 (+3.1)

(2025) and fine-tuned Qwen3VL-4B to predict these action tokens autoregressively (formatting it as a QA task). We then either freeze or unfreeze the vision encoder during VLM fine-tuning, and use the fine-tuned VLM as the backbone initialization for VLA training (also freeze or unfreeze the vision encoder). The test results are shown in the table below.

The results reveal a critical insight. Even when training on real-world images (where there is no sim-to-real visual gap), keeping the vision encoder frozen (Row *Freeze Vision FT*) fails to improve downstream performance. The VLM’s native visual features—despite being *real-world* are insufficient for control. When we allow the vision encoder to update on real-world control data (Row *Unfreeze Vision FT*), performance improves dramatically. This demonstrates that the necessity of fine-tuning the vision encoder is not primarily a confounding variable caused by simulation artifacts. Instead, we consider it to be driven by a semantic gap: the visual features optimized for multimodal understanding or reasoning are not inherently aligned with the fine-grained representations required for low-level manipulation, regardless of whether the images are real or simulated.

Interestingly, this conclusion also partially explains the phenomena observed in Sec. 4.2—namely, why various embodied VQA tasks, whether designed in simulation or in the real world, fail to improve a VLM’s performance on VLA.

However, the visual gap between VLMs and VLAs does not imply that VLM pretraining is unhelpful for VLAs. In Table 8 of the Appendix A.2.5, we observe that training VLAs from scratch leads to performance collapse on Calvin and Simpler, indicating that VLM pretraining is crucial for VLA generalization. Integrating the above analysis, we arrive at the conclusion illustrated in Figure 5. From a feature-learning perspective, the overall spatial direction of representation learning in VLM training broadly aligns with that of VLA training. Nevertheless, around a certain point in training, the two trajectories diverge into different regions, which gives rise to the latent gap currently observed between VLMs and VLAs. This explains why VLM pretraining is indispensable for VLAs, yet a pronounced gap persists between the two.

5 CONCLUSIONS

In this paper, we investigated the impact of various VLMs—including the effect of auxiliary fine-tuning tasks—on the performance of VLA models. Through over 100 training and evaluation experiments conducted across three distinct environments, we assessed the capabilities of nine models and eight categories of auxiliary data for executing manipulation tasks. Our findings offer practical recommendations and a performance reference for the community. A core insight from our study is the significant gap between the capabilities of current VLMs and the demands of VLA embodied tasks. Specifically, we observe a notable discrepancy between a VLM’s performance on standard VQA benchmarks and its actual effectiveness when deployed in a VLA.

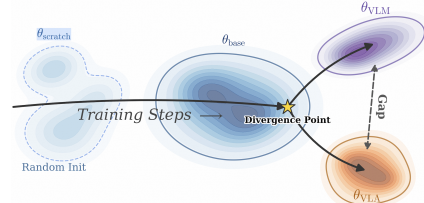


Figure 5: During learning, VLMs and VLAs initially follow the same trajectory. At a certain timestep, they diverge into different regions that cause the gap.

A limitation of our work is the absence of experiments on physical robots. This decision was motivated by challenges related to fairness and reproducibility, as well as difficulties in ensuring test efficiency and fairness across physical hardware setups. We conducted an in-depth experimental analysis of the Real-to-Sim gap and found that the visual discrepancy between VLMs and VLAs likely arises from the inherent heterogeneity between vision–language tasks and low-level action control tasks, rather than merely from a simple image-level sim-to-real gap. This issue is universal across both simulation and real-robot settings. From this perspective, while real-world deployment remains the ultimate goal, we believe that our comprehensive results across multiple, diverse simulation benchmarks provide valuable insights that can inspire and guide future research in this area.

REFERENCES

Shuai Bai, Yuxuan Cai, Ruizhe Chen, Keqin Chen, Xionghui Chen, Zesen Cheng, Lianghao Deng, Wei Ding, Chang Gao, Chunjiang Ge, et al. Qwen3-vl technical report. *arXiv preprint arXiv:2511.21631*, 2025a.

Shuai Bai, Keqin Chen, Xuejing Liu, Jialin Wang, Wenbin Ge, Sibo Song, Kai Dang, Peng Wang, Shijie Wang, Jun Tang, et al. Qwen2. 5-vl technical report. *arXiv preprint arXiv:2502.13923*, 2025b.

Lucas Beyer, Andreas Steiner, André Susano Pinto, Alexander Kolesnikov, Xiao Wang, Daniel Salz, Maxim Neumann, Ibrahim Alabdulmohsin, Michael Tschannen, Emanuele Bugliarello, et al. Paligemma: A versatile 3b vlm for transfer. *arXiv preprint arXiv:2407.07726*, 2024.

Kevin Black, Noah Brown, Danny Driess, Adnan Esmail, Michael Equi, Chelsea Finn, Niccolò Fusai, Lachy Groom, Karol Hausman, Brian Ichter, et al. pi_0: A vision–language–action flow model for general robot control. *arXiv preprint arXiv:2410.24164*, 2024.

Anthony Brohan, Noah Brown, Justice Carbajal, Yevgen Chebotar, Xi Chen, Krzysztof Choromanski, Tianli Ding, Danny Driess, Avinava Dubey, Chelsea Finn, et al. Rt-2: Vision–language–action models transfer web knowledge to robotic control. *arXiv preprint arXiv:2307.15818*, 2023.

Boyuan Chen, Zhuo Xu, Sean Kirmani, Brian Ichter, Dorsa Sadigh, Leonidas Guibas, and Fei Xia. Spatialvlm: Endowing vision–language models with spatial reasoning capabilities. In *Proceedings of the IEEE/CVF Conference on Computer Vision and Pattern Recognition*, pp. 14455–14465, 2024.

Jiuhai Chen, Zhiyang Xu, Xichen Pan, Yushi Hu, Can Qin, Tom Goldstein, Lifu Huang, Tianyi Zhou, Saining Xie, Silvio Savarese, et al. Blip3-o: A family of fully open unified multimodal models–architecture, training and dataset. *arXiv preprint arXiv:2505.09568*, 2025a.

Kaiyuan Chen, Shuangyu Xie, Zehan Ma, and Ken Goldberg. Robo2vlm: Visual question answering from large-scale in-the-wild robot manipulation datasets, 2025b. URL <https://arxiv.org/abs/2505.15517>.

Xiaoyu Chen, Hangxing Wei, Pushi Zhang, Chuheng Zhang, Kaixin Wang, Yanjiang Guo, Rushuai Yang, Yucen Wang, Xinquan Xiao, Li Zhao, et al. Villa-x: enhancing latent action modeling in vision–language–action models. *arXiv preprint arXiv:2507.23682*, 2025c.

Can Cui, Pengxiang Ding, Wenxuan Song, Shuanghao Bai, Xinyang Tong, Zirui Ge, Runze Suo, Wanqi Zhou, Yang Liu, Bofang Jia, et al. Openhelix: A short survey, empirical analysis, and open-source dual-system vla model for robotic manipulation. *arXiv preprint arXiv:2505.03912*, 2025.

Wenliang Dai, Junnan Li, Dongxu Li, Anthony Meng Huat Tiong, Junqi Zhao, Weisheng Wang, Boyang Li, Pascale N Fung, and Steven Hoi. Instructblip: Towards general-purpose vision–language models with instruction tuning. *Advances in Neural Information Processing Systems*, 36, 2024.

Chaorui Deng, Deyao Zhu, Kunchang Li, Chenhui Gou, Feng Li, Zeyu Wang, Shu Zhong, Weihao Yu, Xiaonan Nie, Ziang Song, et al. Emerging properties in unified multimodal pretraining. *arXiv preprint arXiv:2505.14683*, 2025.

Danny Driess, Jost Tobias Springenberg, Brian Ichter, Lili Yu, Adrian Li-Bell, Karl Pertsch, Allen Z Ren, Homer Walke, Quan Vuong, Lucy Xiaoyang Shi, et al. Knowledge insulating vision-language-action models: Train fast, run fast, generalize better. *arXiv preprint arXiv:2505.23705*, 2025.

Mengfei Du, Biniao Wu, Zejun Li, Xuanjing Huang, and Zhongyu Wei. Embspatial-bench: Benchmarking spatial understanding for embodied tasks with large vision-language models. *arXiv preprint arXiv:2406.05756*, 2024.

Qi Feng. Towards visuospatial cognition via hierarchical fusion of visual experts. *arXiv preprint arXiv:2505.12363*, 2025.

Yanjiang Guo, Yucheng Hu, Jianke Zhang, Yen-Jen Wang, Xiaoyu Chen, Chaochao Lu, and Jianyu Chen. Prediction with action: Visual policy learning via joint denoising process. *arXiv preprint arXiv:2411.18179*, 2024.

Yanjiang Guo, Jianke Zhang, Xiaoyu Chen, Xiang Ji, Yen-Jen Wang, Yucheng Hu, and Jianyu Chen. Improving vision-language-action model with online reinforcement learning. *arXiv preprint arXiv:2501.16664*, 2025.

Yucheng Hu, Yanjiang Guo, Pengchao Wang, Xiaoyu Chen, Yen-Jen Wang, Jianke Zhang, Koushil Sreenath, Chaochao Lu, and Jianyu Chen. Video prediction policy: A generalist robot policy with predictive visual representations. *arXiv preprint arXiv:2412.14803*, 2024.

Chi-Pin Huang, Yueh-Hua Wu, Min-Hung Chen, Yu-Chiang Frank Wang, and Fu-En Yang. Thinkact: Vision-language-action reasoning via reinforced visual latent planning. *arXiv preprint arXiv:2507.16815*, 2025.

Physical Intelligence, Kevin Black, Noah Brown, James Darpinian, Karan Dhabalia, Danny Driess, Adnan Esmail, Michael Equi, Chelsea Finn, Niccolo Fusai, et al. pi0.5: a vision-language-action model with open-world generalization. *arXiv preprint arXiv:2504.16054*, 2025.

Moo Jin Kim, Karl Pertsch, Siddharth Karamcheti, Ted Xiao, Ashwin Balakrishna, Suraj Nair, Rafael Rafailov, Ethan Foster, Grace Lam, Pannag Sanketi, Quan Vuong, Thomas Kollar, Benjamin Burchfiel, Russ Tedrake, Dorsa Sadigh, Sergey Levine, Percy Liang, and Chelsea Finn. Openvla: An open-source vision-language-action model. *arXiv preprint arXiv:2406.09246*, 2024.

Xinghang Li, Minghuan Liu, Hanbo Zhang, Cunjun Yu, Jie Xu, Hongtao Wu, Chilam Cheang, Ya Jing, Weinan Zhang, Huaping Liu, et al. Vision-language foundation models as effective robot imitators. *arXiv preprint arXiv:2311.01378*, 2023.

Xuanlin Li, Kyle Hsu, Jiayuan Gu, Karl Pertsch, Oier Mees, Homer Rich Walke, Chuyuan Fu, Ishikaa Lunawat, Isabel Sieh, Sean Kirmani, Sergey Levine, Jiajun Wu, Chelsea Finn, Hao Su, Quan Vuong, and Ted Xiao. Evaluating real-world robot manipulation policies in simulation. *arXiv preprint arXiv:2405.05941*, 2024.

Bo Liu, Yifeng Zhu, Chongkai Gao, Yihao Feng, Qiang Liu, Yuke Zhu, and Peter Stone. Libero: Benchmarking knowledge transfer for lifelong robot learning. *arXiv preprint arXiv:2306.03310*, 2023.

Huaping Liu, Xinghang Li, Peiyan Li, Minghuan Liu, Dong Wang, Jirong Liu, Bingyi Kang, Xiao Ma, Tao Kong, and Hanbo Zhang. Towards generalist robot policies: What matters in building vision-language-action models. *arXiv preprint arXiv:2412.14058*, 2025.

Oier Mees, Lukas Hermann, Erick Rosete-Beas, and Wolfram Burgard. Calvin: A benchmark for language-conditioned policy learning for long-horizon robot manipulation tasks. *IEEE Robotics and Automation Letters (RA-L)*, 7(3):7327–7334, 2022.

Kun Ouyang, Yuanxin Liu, Haoning Wu, Yi Liu, Hao Zhou, Jie Zhou, Fandong Meng, and Xu Sun. Spacer: Reinforcing mllms in video spatial reasoning. *arXiv preprint arXiv:2504.01805*, 2025.

Zhiliang Peng, Wenhui Wang, Li Dong, Yaru Hao, Shaohan Huang, Shuming Ma, and Furu Wei. Kosmos-2: Grounding multimodal large language models to the world. *arXiv preprint arXiv:2306.14824*, 2023.

Karl Pertsch, Kyle Stachowicz, Brian Ichter, Danny Driess, Suraj Nair, Quan Vuong, Oier Mees, Chelsea Finn, and Sergey Levine. Fast: Efficient action tokenization for vision-language-action models. *arXiv preprint arXiv:2501.09747*, 2025.

Krishan Rana, Jesse Haviland, Sourav Garg, Jad Abou-Chakra, Ian Reid, and Niko Suenderhauf. Sayplan: Grounding large language models using 3d scene graphs for scalable task planning. *arXiv preprint arXiv:2307.06135*, 2023.

Pierre Sermanet, Tianli Ding, Jeffrey Zhao, Fei Xia, Debidatta Dwibedi, Keerthana Gopalakrishnan, Christine Chan, Gabriel Dulac-Arnold, Sharath Maddineni, Nikhil J Joshi, et al. Robovqa: Multimodal long-horizon reasoning for robotics. In *2024 IEEE International Conference on Robotics and Automation (ICRA)*, pp. 645–652. IEEE, 2024.

Yide Shentu, Philipp Wu, Aravind Rajeswaran, and Pieter Abbeel. From llms to actions: Latent codes as bridges in hierarchical robot control. In *2024 IEEE/RSJ International Conference on Intelligent Robots and Systems (IROS)*, pp. 8539–8546. IEEE, 2024.

Hao Shi, Bin Xie, Yingfei Liu, Lin Sun, Fengrong Liu, Tiancai Wang, Erjin Zhou, Haoqiang Fan, Xiangyu Zhang, and Gao Huang. Memoryvla: Perceptual-cognitive memory in vision-language-action models for robotic manipulation. *arXiv preprint arXiv:2508.19236*, 2025.

Andreas Steiner, André Susano Pinto, Michael Tschannen, Daniel Keysers, Xiao Wang, Yonatan Bitton, Alexey Gritsenko, Matthias Minderer, Anthony Sherbondy, Shangbang Long, et al. Paligemma 2: A family of versatile vlms for transfer. *arXiv preprint arXiv:2412.03555*, 2024.

BAAI RoboBrain Team. Robobrain 2.0 technical report. *arXiv preprint arXiv:2507.02029*, 2025.

Hugo Touvron, Thibaut Lavril, Gautier Izacard, Xavier Martinet, Marie-Anne Lachaux, Timothée Lacroix, Baptiste Rozière, Naman Goyal, Eric Hambro, Faisal Azhar, et al. Llama: Open and efficient foundation language models. *arXiv preprint arXiv:2302.13971*, 2023.

Homer Walke, Kevin Black, Abraham Lee, Moo Jin Kim, Max Du, Chongyi Zheng, Tony Zhao, Philippe Hansen-Estruch, Quan Vuong, Andre He, Vivek Myers, Kuan Fang, Chelsea Finn, and Sergey Levine. Bridgedata v2: A dataset for robot learning at scale. In *Conference on Robot Learning (CoRL)*, 2023.

Weiyun Wang, Zhangwei Gao, Lixin Gu, Hengjun Pu, Long Cui, Xingguang Wei, Zhaoyang Liu, Linglin Jing, Shenglong Ye, Jie Shao, et al. Internvl3. 5: Advancing open-source multimodal models in versatility, reasoning, and efficiency. *arXiv preprint arXiv:2508.18265*, 2025a.

Yuqi Wang, Xinghang Li, Wenxuan Wang, Junbo Zhang, Yingyan Li, Yuntao Chen, Xinlong Wang, and Zhaoxiang Zhang. Unified vision-language-action model. *arXiv preprint arXiv:2506.19850*, 2025b.

Junjie Wen, Yichen Zhu, Jinming Li, Zhibin Tang, Chaomin Shen, and Feifei Feng. Dexvla: Vision-language model with plug-in diffusion expert for general robot control. *arXiv preprint arXiv:2502.05855*, 2025.

Jihan Yang, Shusheng Yang, Anjali W Gupta, Rilyn Han, Li Fei-Fei, and Saining Xie. Thinking in space: How multimodal large language models see, remember, and recall spaces. In *Proceedings of the Computer Vision and Pattern Recognition Conference*, pp. 10632–10643, 2025.

Wentao Yuan, Jiafei Duan, Valts Blukis, Wilbert Pumacay, Ranjay Krishna, Adithyavairavan Murali, Arsalan Mousavian, and Dieter Fox. Robopoint: A vision-language model for spatial affordance prediction for robotics. *arXiv preprint arXiv:2406.10721*, 2024.

Jianke Zhang, Yanjiang Guo, Xiaoyu Chen, Yen-Jen Wang, Yucheng Hu, Chengming Shi, and Jianyu Chen. Hirt: Enhancing robotic control with hierarchical robot transformers. *arXiv preprint arXiv:2410.05273*, 2024.

Jianke Zhang, Yanjiang Guo, Yucheng Hu, Xiaoyu Chen, Xiang Zhu, and Jianyu Chen. Up-vla: A unified understanding and prediction model for embodied agent. *arXiv preprint arXiv:2501.18867*, 2025a.

Jianke Zhang, Yucheng Hu, Yanjiang Guo, Xiaoyu Chen, Yichen Liu, Wanna Chen, Chaochao Lu, and Jianyu Chen. Unicod: Enhancing robot policy via unified continuous and discrete representation learning. *arXiv preprint arXiv:2510.10642*, 2025b.

Tony Z Zhao, Vikash Kumar, Sergey Levine, and Chelsea Finn. Learning fine-grained bimanual manipulation with low-cost hardware. *arXiv preprint arXiv:2304.13705*, 2023.

Ruijie Zheng, Yongyuan Liang, Shuaiyi Huang, Jianfeng Gao, Hal Daumé III, Andrey Kolobov, Furong Huang, and Jianwei Yang. Tracevla: Visual trace prompting enhances spatial-temporal awareness for generalist robotic policies. *arXiv preprint arXiv:2412.10345*, 2024.

Enshen Zhou, Jingkun An, Cheng Chi, Yi Han, Shanyu Rong, Chi Zhang, Pengwei Wang, Zhongyuan Wang, Tiejun Huang, Lu Sheng, et al. Roborefer: Towards spatial referring with reasoning in vision-language models for robotics. *arXiv preprint arXiv:2506.04308*, 2025a.

Zhongyi Zhou, Yichen Zhu, Minjie Zhu, Junjie Wen, Ning Liu, Zhiyuan Xu, Weibin Meng, Ran Cheng, Yixin Peng, Chaomin Shen, et al. Chatvla: Unified multimodal understanding and robot control with vision-language-action model. *arXiv preprint arXiv:2502.14420*, 2025b.

A APPENDIX

A.1 MORE DETAILS ABOUT TESING ENVIRONMENTS

Calvin ABC-D Calvin is a simulation benchmark for various tabletop manipulation tasks. Its dataset consists of four splits (A, B, C, and D), each with different scene configurations (primarily changes in object and scene colors). During testing, the policy is required to complete a sequence of 1–5 tasks. To prevent larger models from merely overfitting to seen color schemes, we adopt the ABC–D setup, where the model is trained on scenes A, B, and C, and tested on scene D. This setup challenges the VLM’s ability to generalize to novel visual scenes. We train the model for 30k steps on the ABC splits and evaluate it on 1000 task sequences, each with a length of 5. We report the average number of successfully completed tasks per sequence.

SimplerEnv Bridge SimplerEnv is a suite of real-to-sim evaluation environments where the policy is trained on real-world data and tested in simulation. The test scenarios are divided into two categories based on the data source: Google Robot (Fractal) and WindowX (Bridge V2). The former has a smaller visual gap between the training and testing domains, where most policies perform well. To better differentiate the performance of various VLM-based policies, we choose the more challenging Bridge split as our evaluation metric. We train for 50k steps on BridgeV2, with validation every 5k steps (for a total of 10 checkpoints). During evaluation, we run 24 trials with random initializations for each of the four scenes (Pick Carrot, Pick Eggplant, Pick Spoon, and Stack Cube) and calculate the success rate. We report the best result from the validation checkpoints.

Libero-Long (-10) Libero is a simulation benchmark for multi-category manipulation tasks on a fixed tabletop, which contains five task suites. We select the most challenging suite, Libero-Long (also known as Libero-10), which consists of 10 long-horizon tasks involving a variety of objects, scenes, and manipulation types.

A.2 MORE IMPLEMENTATION DETAILS

A.2.1 TRAINING SETUPS

To ensure a fair comparison, we fine-tune the Vision-Language Model (VLM) and the action policy with identical hyperparameters and model configurations in each test environment. Specifically, all experiments of dense VLMs are conducted on 8 NVIDIA A100 GPUs. For Qwen3VL-30B-A3B, we take use of 32 NVIDIA A100 GPUs. All models use a single-view image of the current frame as its visual input and does not take state information as input, which prevents the model from directly learning actions from the state. We fine-tune all parameters of the VLM, including the vision encoder, token embeddings, and the LLM part. The detailed training hyperparameters are as follows:

- **Calvin:** We use a batch size of 128, a learning rate of 2×10^{-5} for all models, and an action chunk size of 10.
- **Simpler & Libero:** We use a batch size of 512, a uniform learning rate of 5×10^{-5} , and an action chunk size of 4.

A.2.2 ABOUT CHOICE OF HYPERPARAMETERS

Here, we provide additional details on hyperparameter choices (action chunk, learning rate, and batch size) and discuss the implications of using exactly the same hyperparameters across all methods.

For all reported results, we perform a sweep on different action chunk sizes during evaluation. We also use different checkpoints to mitigate the training instability. We report the best performance among these runs. In most cases, the best performance was achieved before the final checkpoint, indicating that the models had already converged. The protocol that uses the same hyperparameters ensures that our results reflect each model’s peak capability (convergence), effectively decoupling performance from training proficiency or randomness.

To verify the robustness of our Learning Rate (LR) choice, we performed a sweep using values $\{1e-5, 2e-5, 5e-5, 1e-4\}$ on representative models (Qwen2.5-VL-3B, Qwen2.5-VL-7B, and PaliGemma-1). As shown in the table below, while minor fluctuations exist, the downstream

performance remains highly stable across this range, and the relative ranking of models remains consistent.

Learning Rate	1e-5	2e-5	5e-5	1e-4
Qwen2.5VL-3B	3.844	3.856	3.832	3.792
Qwen2.5VL-7B	4.050	4.057	4.027	3.986
Paligemma-1	3.506	3.506	3.487	3.492

Table 5: Performance across learning rates on Calvin ABC-D.

Regarding batch size, we maximized this parameter uniformly across all models and make sure this stays the same. We believe that larger batch sizes benefit all architectures by stabilizing gradients; therefore, enforcing a large, identical batch size prevents any model from being disadvantaged by gradient noise.

A.2.3 LANGUAGE PROMPTS AND FORMAT

For fair comparison between different VLMs, we prompt all models with the simplest format of prompts while keeping consistent with the VLM’s pretraining prompt format. The detailed prompts for the different VLMs used in VLM4VLA are as follows (including special tokens). For convenience, here we use the robotic instruction `pick up cube` as an example of an input encoded in this manner.

Paligemma-1 & Paligemma-2

The `Paligemma` model employs a `prefix-suffix` encoding scheme during its pre-training. In this scheme, the prefix part is processed with bidirectional attention, while the suffix part uses unidirectional (causal) attention for generative tasks. The two parts are demarcated by a `<bos>` token. For our implementation, we adopt the prefix encoding scheme for image tokens and the suffix encoding scheme for text tokens, as this aligns with the model’s generative training objective.

` ... <bos>pick up cube\n<ActionQuery>`

Kosmos-2

`Kosmos` is a VLM optimized for *grounding* tasks, where its training sequences contain multiple task-specific tokens. Since the action output of a VLA is not a grounding task, we do not include these additional task tokens in our input. The expectation is that the model will automatically learn to leverage its skills acquired from other tasks during the fine-tuning process.

`<s><image> ... </image><p>pick up cube\n</p><ActionQuery>`

Qwen2.5VL (2 models) & Qwen3VL (4 models)

For the `Qwen` series of models, which are instruction-fine-tuned, general-purpose conversational models, an input format that closely mirrors their training would necessitate the inclusion of both system and user prompts. We therefore compared two distinct token concatenation schemes:

- **Scheme 1 (Full Compliance):** This approach strictly adheres to the instruction-SFT format. While this ensures maximum alignment with the model’s pre-training, it results in a longer input token sequence:

`<|im_start|>system\nYou are a helpful assistant.<|im_end|>\n<|im_start|>user\n<|vision_start|> ... <|vision_end|>What action should the robotic arm take to pick up cube<|im_end|>\n<|im_start|>assistant\n<ActionQuery>`

- **Scheme 2 (Simplified Consistency):** This scheme aligns with the simplified approach we used for `Kosmos` and `Paligemma`. It omits the extraneous conversational prompts (e.g., system and user roles) and includes only the most essential special tokens required for sequence construction:

`<|im_start|><|vision_start|> ... <|vision_end|>pick up cube\n<ActionQuery>`

	Prompt	Calvin ABC-D \uparrow	SimplerBridge \uparrow
Qwen2.5VL-3B	Long	3.856	48.00
Qwen2.5VL-3B	Short	3.844 (-0.012)	46.75 (-1.25)
Qwen2.5VL-7B	Long	4.057	46.75
Qwen2.5VL-7B	Short	3.947 (-0.110)	44.00 (-2.75)

Table 6: Comparison between different prompt formats. `Long` prompt denotes Scheme 1, while the `Short` prompt denote the Scheme 2.

The comparison in Table 6 indicates that prompts perfectly matching the Supervised Fine-Tuning (SFT) format perform marginally better than their minimal counterparts. Consequently, we consistently apply the Scheme 1 prompt style to the *QwenVL* series in our remaining experiments to maintain alignment with their original training formats.

A.2.4 INFLUENCE OF IMAGE RESOLUTION

We investigate the impact of image resolution on the final performance. Besides the default settings of 224x224, we conduct higher-resolution experiments on Qwen2.5VL-3B and Qwen2.5VL-7B. Specifically, during VLA training, we set the input image resolution to 224, 512, and 768, respectively, and evaluated on the Calvin ABC-D task under both settings: freezing and not freezing the vision encoder. The results are as follows.

	224x224	512x512	768x768
Qwen2.5VL-3B	3.856	3.832	3.836
+ freeze vision encoder	2.855 (-1.001)	2.749 (-1.083)	2.715 (-1.121)
Qwen2.5VL-7B	4.057	4.062	3.998
+ freeze vision encoder	2.823 (-1.234)	2.746 (-1.316)	2.693 (-1.305)

Table 7: Comparison between different image resolution under freezing or unfreezing vision encoder.

As shown in the table, simply increasing the input resolution (from 224 to 768) did not significantly improve VLA performance when the encoder is fine-tuned. These results suggest that the necessity of fine-tuning is not merely a compensation for low resolution. However, the performance degradation caused by freezing the encoder became more pronounced at higher resolutions (e.g., the gap widens from -1.00 to -1.12 for the 3B model). A plausible explanation is that higher resolution and more frozen visual tokens may lead to spurious correlation, which incurs additional performance losses.

A.2.5 LOWER BOUND OF TRAINING FROM SCRATCH

To isolate the contribution of the VLM backbone, we establish a lower-bound baseline by training VLM4VLA variants entirely from random initialization. This clarifies whether the observed generalization stems from the architecture alone or from VLM pre-training. We train Qwen2.5-VL (3B and 7B) and PaliGemma from scratch on the Calvin ABC-D and Simpler-Bridge benchmarks. We strictly match the training hyperparameters and evaluation protocols reported in the main paper for all from-scratch runs.

As shown in Table 8, models trained from scratch exhibit substantial degradation across both benchmarks and all model sizes. This gap indicates that VLM pre-training is fundamental to the generalization ability of the VLA model, beyond architectural design. Training from scratch yields markedly lower performance, confirming that VLM pre-training is a prerequisite for strong downstream generalization in VLM4VLA.

A.2.6 IMPLEMENTATION DETAILS ABOUT VLM4VLA ARCHITECHTURE

We provide the detailed model architechture in Table 9. We maintain a consistent architecture for the action-specific modules across all models, including a fixed number of learnable tokens and a

Table 8: Performance of training from scratch compared to pretrained initialization. We report absolute scores and the change (in parentheses) relative to pretrained models on Calvin ABC-D and Simpler-Bridge.

Model	Calvin ABC-D	Simpler-Bridge
Qwen2.5VL-3B + from scratch	3.856 1.381 (-2.475)	48.00 15.75 (-32.25)
Qwen2.5VL-7B + from scratch	4.057 1.769 (-2.288)	46.75 18.20 (-28.75)
Paligemma-1 + from scratch	3.506 1.129 (-2.377)	55.25 14.50 (-40.75)

uniform hidden size for the action head. Consequently, the variation in the number of additional trainable parameters is solely dependent on the VLM’s native `hidden_size`. The Policy Head architecture presented here omits the final linear layer, which maps the features to the action space (i.e., `Linear(1024, 7)`).

VLM	Backbone Size	Policy Head Size	Learnable Tokens	LLM Hidden Size	Policy Head
Qwen2.5VL-3B	3755M	6.58M	1	2048	Linear(2048, 1024) ReLU Linear(1024, 1024)
Qwen2.5VL-7B	8292M	11.69M	1	3584	Linear(3584, 1792) ReLU Linear(1792, 1024)
Qwen3VL-2B	2128M	6.58M	1	2048	Linear(2048, 1024) ReLU Linear(1024, 1024)
Qwen3VL-4B	4437M	8.02M	1	2560	Linear(2560, 1280) ReLU Linear(1280, 1024)
Qwen3VL-8B	8767M	13.92M	1	4096	Linear(4096, 2048) ReLU Linear(2048, 1024)
Qwen3VL-30B-A3B	31071M	6.58M	1	2048	Linear(2048, 1024) ReLU Linear(1024, 1024)
Paligemma-1	2923M	6.58M	1	2048	Linear(2048, 1024) ReLU Linear(1024, 1024)
Paligemma-2	3032M	7.27M	1	2304	Linear(2304, 1502) ReLU Linear(1502, 1024)
KosMos-2	1664M	6.58M	1	2048	Linear(2048, 1024) ReLU Linear(1024, 1024)

Table 9: Detailed architecture of different VLM4VLA backbones.

A.3 IMPLEMENTATION AND EVALUATION DETAILS FOR THE PI0

Reproducing pi0 In our experiments, we reproduced the `pi0` model to serve as a strong comparative baseline. We leveraged the model implementation from the official code released by Allen but excluded its proprioceptive input module. Specifically, we integrated the `pi0` model architecture into the **VLM4VLA** data-loading and training framework for fine-tuning and evaluation. This model-only migration was a deliberate choice, as we observed that the data preprocessing strategies and pretraining data used in the original `pi0` implementation were inconsistent with those of OpenVLA and our **VLM4VLA** framework, thus ensuring a fairer comparison.

Modification of the Proprioceptive State Expert We modified the state expert in `pi0` by directly concatenating the outputs of the VLM expert and the action expert. Since the state and action experts in the original `pi0` architecture share the same parameters, our modification only alters the model’s input pathway without changing its underlying structure or parameter count.

Evaluation Protocol During our experiments, we discovered that the Flow-matching loss used in `pi0` leads to significant performance instability. Specifically, multiple rollouts of the same `pi0` policy in an identical starting environment could yield success rate fluctuations as high as $\pm 20\%$. In stark contrast, our **VLM4VLA** approach is deterministic under the same conditions, producing identical outcomes for each run without stochasticity. This high variance necessitated a more extensive evaluation rollouts for `pi0` to obtain a reliable estimate of its true performance. Consequently, when testing `pi0`, we performed a greater number of rollouts for each checkpoint under various settings:

- Calvin: We averaged the results over 3 evaluation runs per model.
- Simpler: We performed 240 evaluation runs for each model on every task.
- Libero: We performed 250 evaluation runs for each model on every task.

A.4 CORRELATION ANALYSIS BETWEEN VLM CAPABILITY AND VLA PERFORMANCE

Here we provide a detailed explanation of how the data points in Figure 3 are obtained and what each graphical element represents.

- The x-axis represents the general capability of different VLMs.
- Each set of three vertically aligned points with the same color corresponds to the results of the same VLM used as the VLM4VLA backbone across three benchmarks.
- Marker shapes denote benchmarks: circles for SimplerEnv, triangles for LIBERO, and squares for CALVIN (see the legend on the right).
- The three colored lines are linear fits to the points from each benchmark: red for Simpler (fit over circle markers), blue for LIBERO (fit over triangle markers), and green for CALVIN (fit over square markers).

Figure 3 uses VLMs from data sourced from the experiments reported in Tables 1 and 2. We elaborate how we evaluate different VLMs in terms of their general capabilities. QwenVL are general-purpose VLMs that have been evaluated across a wide range of multimodal understanding benchmarks. We take the average of their officially reported results on a set of multimodal general, reasoning, text, grounding, agentic, and embodied benchmarks as the x-axis value. This set includes: MMBench v1.1 (en), MMStar, BLINK, HallusionBench, AI2D, OCRBench, MVBench, VideoMME, MMMU, MathVista, MathVision, CountBenchQA, RefCOCO (all), GPQA, OmniSpatial, RealWorldQA, ERQA, and VSI-Bench. For PaliGemma and Kosmos, which are not trained for general-purpose tasks, we use their performance on their respective specialized evaluation suites as the metric. Specifically, PaliGemma is evaluated on RefCOCO (all), AI2D, CountBenchQA, and GQA; Kosmos is a grounding-focused VLM, which uses only RefCOCO results as its metric. Because the latter two models are evaluated on a subset of the tasks used for the former two (reflecting their lack of general-task capability), we apply a downweighting to their scores. This yields an approximate assessment of the “general capability of different types of VLMs” as a reference.

To quantify the strength of the linear relationship between each benchmark and VLM capability, we report the correlation metrics for the three fitted lines (Pearson correlation coefficient r and R^2):

VLM4VLA Baseline	Task-1	Task-2	Task-3	Task-4	Task-5	ALL↑
Qwen2.5VL-3B	0.922	0.842	0.766	0.700	0.626	3.856
+ Robopoint	0.924	0.829	0.749	0.683	0.598	3.783 (-0.073)
+ Vica332k	0.940	0.842	0.758	0.692	0.615	3.847 (-0.009)
+ Bridgeeqva	0.945	0.843	0.744	0.657	0.577	3.765 (-0.091)
+ Robo2vIm	0.925	0.833	0.737	0.668	0.597	3.760 (-0.096)
Qwen2.5VL-7B	0.935	0.864	0.807	0.758	0.693	4.057
+ Robobrain2	0.938	0.849	0.767	0.704	0.629	3.887 (-0.170)
+ Omni-Generation	0.928	0.833	0.760	0.711	0.654	3.876 (-0.181)
+ VQA-Mix	0.938	0.856	0.794	0.732	0.658	3.978 (-0.079)

Table 10: Comparison of different Embodied VQA finetuning on VLM4VLA (best results on each settings)

- Calvin: $r = 0.839, R^2 = 0.703$
- SimplerEnv: $r = -0.358, R^2 = 0.128$
- Libero: $r = -0.194, R^2 = 0.038$

A.5 DETAILED RESULTS OF AUXILIARY TASKS

The results on each finetuned VLM on VLA tasks (Calvin ABC-D) are shown in Table 10 (corresponding to Chart 4).

A.6 DETAILS ABOUT DATASETS USED FOR FINETUNING VLM

Robopoint (Yuan et al., 2024) A pointing task dataset collected in a simulator. Given an image and a target location, the model is required to output the 2D coordinates that satisfy the target requirement. This finetuning dataset contains 1.432M samples. As shown in the table, after finetuning, the performance of Qwen2.5VL-3B on the pointing task improved by $\sim 20\%$ on the test split.

Vica-332k (Feng, 2025) A spatial understanding dataset constructed from RGB-D datasets. It covers a wide range of capabilities, including size estimation, position understanding, distance estimation, and so on. After finetuning Qwen2.5VL-3B on this dataset, we achieve a performance improvement of $\sim 15\%$ on VSI-Bench Yang et al. (2025).

Bridgevqa We used VQASynth to annotate data from Bridge-v2, Fractal, and Calvin ABC, combining them into a spatial understanding question-answering dataset. The main QA content includes judging the distance, size, and depth between two objects.

Robo2vIm (Chen et al., 2025b) An action-oriented question-answering dataset built from 176k real robot trajectories, containing 667k VQA pairs. It involves tasks such as multi-view understanding, success prediction, position management, and trajectory judgment. After finetuning Qwen2.5VL-3B on this dataset, we achieved a 60% performance improvement on its test set.

Robobrain2 (Team, 2025) A large-scale embodied VQA dataset and a VLM finetuned on Qwen2.5VL-7B. The tasks include pointing, planning, and marking trajectory. We directly use their finetuned VLM as the backbone for our VLM4VLA.

Omni-Generation Qwen-vlo integrates a diffusion model into VLM and trains on both image generation, depth map generation, and semantic segmentation map generation tasks. We use the resulting VLM part (Qwen2.5VL-7B as the backbone for VLM4VLA).

VQA-Mix We mix the aforementioned VQA datasets with other large-scale general VQA data to finetune Qwen2.5VL-7B. The embodied related tasks include approximately 620k image-text pairs, including Vica Feng (2025), SpaceR Ouyang et al. (2025), Embsspatial Du et al. (2024) and Refspatial Zhou et al. (2025a). The general VQA data consists of 360k QA pairs.



Example of Robopoint Data

Question: Locate several points on an item situated beneath the bordered item.

Answer: $[(0.56, 0.69), (0.53, 0.76), (0.45, 0.72), (0.43, 0.67)]$



Example of Vica Data

Question: How large is this room in terms of square meters? If more than one room is shown, approximate the overall space.

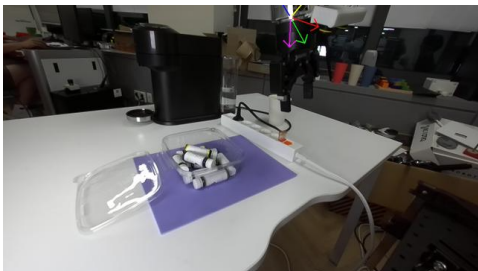
Answer: 18.33



Example of Bridgevqa Data

Question: Who is positioned more to the left, the red spoon or the robot arm?

Answer: Red spoon is more to the left.



Example of Robo2VLM Data

Question: The robot task is to flip the switch of the extension cord. Which colored arrow correctly shows the direction the robot will move next?
Choices: A. Yellow. B. Blue. C. None of the above. D. Purple. E. Green. Please answer directly with only the letter of the correct option and nothing else.

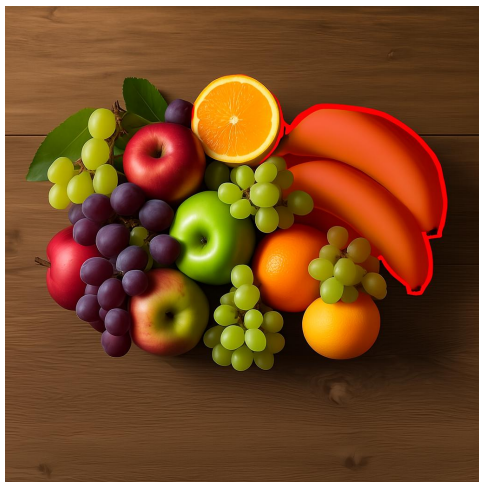
Answer: C



Example of Robobrain Data (ShareRobot)

Question: reach for the ketchup bottle

Answer: $[[113.66,106.19],[153.30,111.42], [217.61,121.14],[248.27,135.35]]$



Example of Omni-Generation Tasks

Question: Use a red mask to segment the edges of the banana in the image.

Answer: Generated mask in the image.